Solid Earth Discuss., https://doi.org/10.5194/se-2019-73
Manuscript under review for journal Solid Earth
Discussion started: 23 April 2019

Solid Earth
Discussions

The impact of rheological uncertainty on dynamic topography predictions: Gearing up for dynamic topography models consistent with observations

Ömer F. Bodur, Patrice F. Rey

EarthByte Group, School of Geosciences, The University of Sydney, NSW 2006, Australia,

Correspondence to: Ömer F. Bodur (omer.bodur@sydney.edu.au)

Abstract

Much effort has been given on extracting the dynamic component of the Earth's topography, which is driven by density heterogeneities in the mantle. Seismically mapped density anomalies have been used as an input into mantle convection models to predict the present-day mantle flow and stresses applied on the Earth's surface, resulting in dynamic topography. However, mantle convection models give dynamic topographies generally larger by a factor of ~2 compared to dynamic topographies estimated from residual topography after extraction of the isostatically compensated topography. Our 3D thermo-mechanical numerical experiments suggest that this discrepancy can be explained by the use of a viscosity model, which doesn't account for non-linear viscosity behaviour. In this paper, we numerically model the dynamic topography induced by a spherical density anomaly embedded into the mantle. When we use non-linear viscosities, our numerical models predict dynamic topographies lesser by a factor of ~2 than those derived from numerical models using isoviscous rheology. This reduction in dynamic topography is explained by either the formation of a low viscosity channel beneath the lithosphere, or a decrease in thickness of the mechanical lithosphere due to induced local reduction in viscosity. Furthermore, we show that uncertainties related to activation volume and fluid activity lead to variations in dynamic topography of about 20%.

1. Introduction

The Earth's mantle is continuously stirred by hot upwellings from the core-mantle boundary, and by subduction of colder plates from surface into the deep mantle (Pekeris, 1935; Isacks et al., 1968; Molnar and Tapponnier, 1975; Stern, 2002). This introduces temperature and density anomalies that stimulate mantle flow and forces dynamic uplift or subsidence at the plates' surface (Gurnis et al., 2000; Braun, 2010; Moucha and Forte, 2011; Flament et al., 2013). Dynamic topography can affect the entire planet's surface with varying magnitudes. Because it is typically a low-amplitude and long-wavelength transient signal, it is often dwarfed by topography created by plate tectonic processes. Therefore, investigations on dynamic topography signals mostly focus on non-tectonic regions where the dynamic topography can be extracted from the subsidence history of sedimentary basins. Dynamic subsidence and uplift events are identified by isolating part of the subsidence that cannot be explained either by thermal relaxation or tectonic processes such as crustal thinning (Sclater and Christie, 1980).

For the present day, the observational constraints on dynamic topography come from residual topography measurements (Hoggard et al., 2016). Residual topography is calculated by removing the isostatic components from the Earth's topography (Crough, 1983; Cazenave et al., 1989; Davies and Pribac, 1993; Steinberger, 2007). Hoggard et al., (2016)'s comprehensive work revealed that residual topography varies between ±500 m at very long-wavelengths (i.e. ~10,000 km) and can increase up to ±1,000 m at shorter wavelengths (i.e. ~1,000 km). However, the accuracy of these estimates depends on our knowledge of the thermal and mechanical structure of the lithosphere. Another approach to constrain present day Earth's dynamic topography involves numerical modelling of present-day mantle flow using seismically mapped density anomalies as an input (Steinberger, 2007; Moucha et al., 2008; Conrad and Husson, 2009). However, this method requires a good knowledge of the viscosity structure in the Earth's interior (Parsons and Daly, 1983; Hager, 1984; Hager et al., 1985; Hager and Clayton, 1989). The problem is that dynamic topography predictions derived from mantle convection models are generally larger by a factor of two than estimates from residual topography (Cowie and Kusznir, 2018; Flament et al., 2013). We hypothesise that this could be related to an oversimplification of the viscous behaviour of the flowing mantle. In this paper, we explore how the magnitude of dynamic topography is impacted when we use a viscosity model in which the viscosity depends on strain rate, temperature, pressure and fluid content. In this paper, we first summarize the well-established analytical solution for calculating dynamic topography induced by a spherical density anomaly embedded into an isoviscous fluid (Morgan, 1965a; Molnar et al., 2015). Then, assuming isoviscous rheology, we illustrate that the amplitude of dynamic topography depends on the viscosity structure of the Earth's interior as shown by (Morgan, 1965a; Molnar et al., 2015). Finally, we use 3-D coupled thermo-mechanical numerical experiments of the Stokes' flow to assess the dependency of dynamic topography to nonlinear rheology using viscosity which depends on temperature, pressure, strain rate and fluid content. We show that more realistic rheology can induce local variations in viscosity and result in lesser magnitude of dynamic topography than those derived from models using isoviscous rheology.

2. Dynamic topography driven by a rising sphere: Analytical and numerical solutions

2.1 Analytical solution for one layer isoviscous fluid

We assume here a simple 2D model representing a very viscous spherical density anomaly embedded into a semi-infinite isoviscous fluid bounded by an upper free surface. Earliest analytical investigations revealed that, albeit counter-intuitive, the magnitude of the induced surface deflection due to the rising sphere is independent of the viscosity of the fluid. The dynamic topography is a function of the vertical total stress (σ_{zz}) applied to the surface which is proportional to the size and depth of the density anomaly according to Equation 1 (Morgan, 1965a, 1965b).

$$\sigma_{zz}(x,0) = [2g\delta\rho r^3]\frac{D^3}{(D^2+x^2)^{5/2}} \text{ (1),}$$

where g is the gravitational acceleration, $\delta\rho$ is density difference between the anomaly and the ambient material, *r* is radius of the sphere, and *D* is distance from the surface to the centre of the anomaly (modified from Morgan 1965a, see Figure 1a). The dynamic topography e_{zz} is given by:

$$e_{zz}(x,0) = \frac{\sigma_{zz\,(x,0)}}{\rho g} \text{ at } z = 0 \text{ (2),}$$

where ρ is mantle density (Morgan, 1965a; Houseman and Hegarty, 1987). In Figure 1a, we plot the dynamic topography induced by a sphere of 1% density anomaly, whose centre is at 372 km depth (*D*= 372 km) below the free surface. We calculate the vertical total stress and convert it to dynamic topography by using Equation 2 for different values of the radius of the sphere. The amplitude of dynamic topography shows an accelerating increase by cubic dependence on the radius of the spherical density anomaly (Fig. 1a, black solid line). For the same problem, Molnar et al., (2015) provided a solution allowing to consider density anomalies of finite viscosity (η_{sphere}) (Eqn. 3):

$$\sigma_{zz}(C,0) = \frac{-\delta\rho r^3 D}{3f}\left[\frac{3-2f}{C^3} + \frac{18(f-1)r^2}{C^5} + \frac{6fD^2}{C^5} - \frac{30(f-1)r^2D^2}{C^7}\right] \text{ (3),}$$

where $C^2=D^2+x^2$ and f = $(\eta_1 + \frac{3\eta_{sphere}}{2})/(\eta_1 + \eta_{sphere})$, for very viscous sphere ($\eta_{sphere} \gg \eta_1$) f=1.5, and deformable sphere ($\eta_{sphere} \cong \eta_1$) f<1.5. In Figure 1a, we give two more plots of dynamic topography where f= 1.5 for hard sphere and f=1.25 for $\eta_{sphere} = \eta_1$ by using Equation 2 and 3. Figure 1a shows that a rising deformable sphere creates higher dynamic topography compared to a very viscous sphere. These show that the viscosity contrast between the spherical anomaly and the surrounding material can affect the dynamic topography. In the section that follows, we explore how dynamic topography varies when there is layering in viscosity, such as existence of a strong lithosphere above the anomaly.

2.2 The impact of layered viscosity structure on dynamic topography

A more generalized solution has been put forward to accommodate the presence of a stronger upper layer representing the lithosphere (η_2) above a lower weaker layer representing the convective mantle (η_1, with $\eta_1 < \eta_2$ in Fig. 1b). In this case, Morgan (1965a) showed (Eqn. 4) that the normal total stress induced by the density anomaly at depth is dependent on the mass anomaly per unit length (M_u), its depth (D), and marginally on the ratio of the viscosity of the convective mantle to the viscosity of the lithosphere ($R=\eta_1/\eta_2$).

$$\sigma_{zz}(x,0) = \int_0^{\infty} \sigma_n \cos nx \ dn \quad (4),$$

where

$$\sigma_n = \frac{M_u g e^{-n(D-d)}}{2\pi(RS_h + C_h)}\left\{1 + n(D-d) + nd\left[\frac{1 - nD + n(D-d)(RC_h + S_h)/(RS_h + C_h)}{1 + nd(1-R^2)/(RS_h + C_h)(RS_h + S_h)}\right]\right\}$$

and $C_h = \cosh nd$, and $S_h = \sinh nd$ (n is wave number) and d is the upper layer thickness (modified from Morgan 1965a). Following Morgan (1965a), Figure 1b illustrates the relative importance of R as well as the ratio of the thickness of the upper layer to the depth of the anomaly (d/D). As long as the lithosphere is more viscous than the asthenosphere, the vertical total stress at the surface has a minor dependence on the viscosity of the lithosphere (see solid lines with R=1 and R=0.01 in Fig. 1b). Figure 1b also shows that the magnitude of dynamic topography increases as the density anomaly is brought closer to the surface (compare solid black line with R=1 and dashed black line with R=1). Moreover, its sensitivity on the relative viscosity of the lithosphere also increases. Under the assumption where the lithosphere is less viscous than the asthenosphere, the normal stress is much reduced and is strongly dependent

Solid Earth Discuss., https://doi.org/10.5194/se-2019-73
Manuscript under review for journal Solid Earth
Discussion started: 23 April 2019

on the viscosity of the lithosphere (Fig. 1b). These demonstrate that layering in viscosity can have strong impact on the amplitude of dynamic topography. In the next section, we use analytical solutions above to benchmark a numerical model, which we will then extend to non-linear viscosity.

2.3 Numerical solutions

For comparison with analytical solutions (Morgan, 1965a; Molnar et al., 2015), we consider 3D numerical models involving 1, 2 and 3 isoviscous layers. These benchmark experiments will be used as references for the non-isoviscous models in section 3. Taking advantage of the symmetry of the experimental setup, we extract viscosity and velocity fields along a 2D cross section passing through the centre of the thermal anomaly, from which we get streamlines and vertical velocity profile along the vertical axis at the centre of the models. We calculate the dynamic topography from the normal stress computed at the surface. We use the open-source code Underworld which solves the Stokes' equation at insignificant Reynolds value (Moresi et al., 2003, 2007). The 3D computational grid represents a domain 3,840 km x 3,840 km x 576 km with a resolution of 6 km along the vertical z axis and 10 km along the x and y axes (Fig. 2). In all experiments, we include a 42 km thick continental crust above the upper mantle. The density structure (see Table 1 for all parameters thermal parameters) is sensitive to the geotherm via a coefficient of thermal expansion and compressibility. The geotherm is defined using a radiogenic heat production in the crust, a constant temperature of 20ºC at the surface, and a constant temperature of 1,350ºC at 150 km. We disregard the adiabatic heating and the asthenosphere is kept at 1,350ºC. At a depth of 372 km below the surface, we embed a positive spherical temperature anomaly of +324ºC which delivers a 1% volumetric density difference. The radius of the sphere is 96 km. In all experiments, we impose free slip velocity boundary conditions at all walls, such as V_x and V_y are set to be free, but V_z=0 cm yr^{-1} at the top wall.

2.3.1 Dynamic topography due to a rising sphere in an isoviscous fluid

In the first experiment (Fig. 3a Experiment 1), we assign the same constant depth-independent viscosity of 10^{21} Pa s to the crust, mantle and the density anomaly. The streamlines for Experiment 1 (Fig. 3a) show formation of two convective cells at the sides of the sphere covering the entire crust and mantle. The vertical velocity profile indicates that the thermal anomaly is rising with a peak velocity of ~2.4 cm yr^{-1}, which is faster than the 2.0 cm yr^{-1} predicted by the analytical solution (Fig. 4a). Experiment 1 predicts a dynamic topography of 114 m (Fig 4b) which is lower than 132 m predicted by Molnar et al., (2015)'s analytical solution. We have verified that increasing the depth of our model from 576 km to 864 km increases the dynamic topography from 114 m to 122 metres. Therefore, the misfit in amplitude of dynamic topography arises from the finite space in our numerical experiments compared to the semi-infinite half-space used in the analytical solution. Our numerical experiment using isoviscous material delivers a result globally consistent with the analytical solutions of Morgan (1965a) and Molnar et al., (2015).

2.3.2 Dynamic topography on a strong lithosphere above an isoviscous asthenosphere

In Experiment 2, we assign to the lithosphere a constant viscosity 100 times larger (i.e. 10^{23} Pa s) than that of the asthenosphere (i.e. 10^{21} Pa s, Fig. 3b). This layering results in a decrease in thickness of the asthenosphere. As a result, the convective cells are narrower (Fig. 3b). The streamlines are deflected across the lithosphere-asthenosphere boundary due to viscosity contrast (Fig. 3b), and there is a sharp variation in vertical velocity at the base of the lithosphere (Fig. 4a, red solid line). The maximum vertical velocity of ~2.1 cm yr^{-1} is attained near the centre of the anomaly. When compared to Experiment 1, the dynamic topography (Fig. 4b, red solid line) shows a significant increase from ~114 m to ~174 m. This increase is consistent with analytical estimations showing an increase in dynamic topography for the case where viscosity increases toward the surface (see Fig. 1b, R<1). In Experiment 2a (not shown here), we tested a different ratio of thickness of the lithosphere to the depth of the anomaly (see *d/D* in Equation 4) by increasing the lithospheric thickness from 150 km to 200 km, while keeping all parameters identical to those of Experiment 2. As predicted by Eqn. 4, the model gives a dynamic topography of ~191 m, the highest among all experiments (Fig. 4b, red dashed line). Overall, counter-intuitively, the presence of a thick viscous lithosphere enhances the dynamic topography.

2.3.3 The impact of low viscosity channel on the dynamic topography

In Experiment 3 (Fig. 3c), we introduce a third 60 km thick low viscosity layer (i.e. 10^{19} Pa s) beneath the base of the lithosphere. The existence of a low viscosity layer has been suggested by several works (Craig and McKenzie, 1986; Phipps Morgan et al., 1995; Stixrude and Lithgow-Bertelloni, 2005; Becker, 2017). In this experiment, in order to prevent large viscosity contrast that can impede the numerical convergence, the viscosity of the lithosphere and ambient asthenosphere are set as 10^{22} Pa s and 10^{21} Pa s, respectively. When compared to Experiment 1, streamlines indicate a further decrease in size of the convective cells, and more importantly, strong horizontal divergence of the streamlines within the low viscosity layer (Fig. 3c). The vertical velocities are also enhanced in the asthenosphere, and reach up to ~2.8 cm yr^{-1} slightly above the centre of the anomaly (Fig. 4a, orange solid line). When compared to Experiment 1, we observe a strong reduction in dynamic topography (Fig. 4b, orange solid line) from 114 m to 88 m. This is due to the damping effect of the low viscosity channel, which reduces the deviatoric stress through its ability to flow. This low viscosity channel acts as a decoupling layer.

Until now, the viscosities were assumed to be constant. However, results from experimental deformation on mantle aggregates strongly suggest that the viscosity is highly nonlinear (Hirth and Kohlstedt, 2003). In what follows, we explore the influence of more realistic viscosities on dynamic topography.

3. The impact of nonlinear viscosity on dynamic topography

3.1 Viscosity structure of the Earth's interior

Earth's mantle is not isoviscous. Geological records of relative sea level changes related to postglacial rebound, geophysical observations of density anomalies inferred from seismic velocity variations in the mantle and satellite measurements of the longest wavelength components of the Earth's geoid have been used to infer the radial viscosity profile of the Earth's interior (Hager et al., 1985; Forte and Mitrovica, 1996; Mitrovica and Forte, 1997; Kaufmann and Lambeck, 2000). Henceforward, beneath the lithosphere, a variation in viscosity up to two orders of magnitude has been proposed (e.g., Kaufmann and Lambeck, 2000). Investigations of the rheological properties of crustal and mantle rocks via rock deformation experiments revealed a nonlinear dependence of viscosity on applied deviatoric stress, pressure, temperature, grain size and the presence of fluids (Post and Griggs, 1973; Chopra and Paterson, 1984; Karato, 1992; Karato and Wu, 1993; Gleason and

Tullis, 1995; Ranalli, 1995; Hirth and Kohlstedt, 2003; Korenaga and Karato, 2008). These experiments lead to the following relationship:

$$\eta_{eff}(\dot{\varepsilon}, P, T) = A^{\left(\frac{-1}{n}\right)} d^{\left(\frac{p}{n}\right)} f_{H_2O}{}^{\left(\frac{-r}{n}\right)} \dot{\varepsilon}^{\left(\frac{1}{n}-1\right)} e^{\left(\frac{Q+PV}{nRT}\right)} \quad (5).$$

where σ, $\dot{\varepsilon}$ and *A* stands for differential stress, strain rate and pre-exponential factor; *p, r* and *n* are exponents for grain size (*d*), water fugacity (f_{H_2O}) and stress, respectively; *V* and *Q* are the energy and volume of activation.

In the case where mantle flow is driven by the temperature difference at the boundary of the convective layer or by internal heating, the dominant strain mechanism is diffusion creep because low deviatoric stresses are expected. However, mantle flow in the vicinity of a moving density anomaly is likely driven by deviatoric stresses that exceed the threshold for dislocation creep. In this case, nonlinear viscosities lead to strong local variation in viscosity in the vicinity of the moving density anomaly. Are those local variations in viscosity important for dynamic topography? To answer this question, we need reasonable constraints on the rheological parameters controlling rocks' viscosity. However, the extrapolation from laboratory strain rates typically in the range of 10^{-6} s^{-1} to 10^{-4} s^{-1} to mantle conditions where strain rates are typically on the order of 10^{-13} s^{-1} results in significant uncertainties on the activation volume, activation energy and stress exponent (Hirth and Kohlstedt, 2003; Korenaga and Karato, 2008). In what follows, we explore how nonlinear viscosity impacts the dynamic topography and address how the uncertainties on the activation volume can affect the dynamic topography.

In Experiments 4 and 5 (Fig. 5), we use published visco-plastic rheological parameters for the crust and mantle, therefore the viscosity depends on temperature, pressure and strain rate as indicated by Equation 5. We use quartzite rheology for the crust (Ranalli, 1995), and test both dry and wet olivine rheologies for the upper mantle (Hirth and Kohlstedt, 2003). Other parameters are identical to those in Experiments 1-3. We give all the rheological and thermal parameters in Table 1. For a particular rheology (i.e. dry or wet) we vary the activation volume by using the minimum and maximum reported values (Hirth and Kohlstedt, 2003).

3.2 Numerical results: the case of dry olivine

In Experiments 4a and 4b, we consider dry dislocation creep of olivine ($n > 1$, $p = 0$, r = 0) in the mantle. The reported activation volume for this rheology varies between 6x10^{-6} m^3 mol^{-1} and 27x10^{-6} m^3 mol^{-1} (Hirth and Kohlstedt, 2003). In Experiment 4a (Fig. 4b), we test the lower value. The streamlines show similar pattern with Experiment 2. Interestingly, the maximum vertical velocity peaks at 75 cm yr^{-1}, near the upper boundary of the sphere (Fig. 6a, black dashed line). This is due to the formation of a low viscosity asthenosphere above the rising sphere (Fig. 5a, Experiment 4a). This experiment gives a dynamic topography of ~149 m (Fig. 6b, black dashed line). It confirms that a strong contrast in viscosity between the lithosphere and asthenosphere enhances the dynamic topography signal. We note that the viscosity contrast is attained by smoother transition between the lithosphere and asthenosphere (Fig. 7a, black dashed line). This also effectively reduces the thickness of the lithosphere below 140 km, which is 150 km thick by the thermal definition (Fig. 7c).

When we increase the activation volume to 27x10^{-6} m^3 mol^{-1}, the convection cells grow much larger and show continuity through the lithosphere (Fig. 5a, Experiment 4b). The sphere has a very low rising speed of ~0.25 cm yr^{-1} (Fig. 6a, black solid line). Compared to Experiment 4a, the dynamic topography shows a strong decrease from ~149 m to ~105 m (Fig. 6b, black solid line). This is an example where the system behaves nearly as a single layer with homogenous viscosity. The near absence of viscosity contrast between the lithosphere and asthenosphere explains the smaller magnitude of the dynamic topography. Moreover, the formation of moderately low viscosity channel (Fig. 7a, black solid line) also contributes to the decrease of the dynamic topography.

3.3 Numerical results: the case of wet olivine

In Experiments 5a and 5b, we consider dislocation creep of wet dry olivine in the mantle. The reported uncertainty in activation volume is between 11x10^{-6} m^{3} mol^{-1} and 33x10^{-6} m^{3} mol^{-1} (Hirth and Kohlstedt, 2003). In Experiment 5a, we test the lower value. The streamlines show similar pattern with Experiment 4a, but with slightly larger convective cells (Fig. 5b, Experiment 5a). The rising speed of the anomaly exceed 140 cm yr^{-1} (Fig. 6a, orange dashed line). This is promoted by the low viscosity region sitting above the rising sphere. The dynamic topography is ~110 m (Fig. 6b, orange dashed line). This is a bit surprising because of the strong (3 orders of magnitude) contrast in viscosity between the lithosphere and asthenosphere. However, Figure 7a shows that thickness of the viscous lithosphere is reduced by about 30 to 45 km in comparison to Experiment 4a (10 – 30 km) which delivered a dynamic topography of ~149 m with same viscosity contrast (Figure 7b,c).

In Experiment 5b, we increase the activation volume from 11x10^{-6} m^{3} mol^{-1} to 33x10^{-6} m^{3} mol^{-1}. The vertical velocities show significant decrease from 140 cm yr^{-1} to 0.34 cm yr^{-1} (Fig. 6a, orange solid line). This is due to an increase in viscosities above the rising sphere. Compared to Experiment 5a, the dynamic topography decreases from ~110 m to ~90 m (Fig. 6b, orange solid line). Compared to Experiment 4b, the dynamic topography is expected to be higher due to slight increase in viscosity contrast (Fig. 7a,b). However, the increase in thickness of the low viscosity channel (Fig. 7a,d) is more effective and thereby causes a greater reduction in magnitude of the dynamic topography.

In summary, experiments using nonlinear rheology generally give lower amplitudes of dynamic topography compared to experiments using isoviscous rheology (Fig. 8). When we use dry olivine rheology for the upper mantle, the dynamic topography varies between ~105 m and ~149 m, whereas under wet conditions, the dynamic topography varies between ~90 m and ~110 m (Fig.8). These variations are due to uncertainties in the activation volume as well as fluid content in olivine rheologies.

4. Discussion and conclusion

By using coupled 3D thermo-mechanical numerical experiments, we model the dynamic topography driven by a rising sphere of 1% density anomaly, having 96 km radius and emplaced at 372 km depth. In line with analytical studies (Morgan, 1965a; Molnar et al., 2015), the experiments show that dynamic topography is sensitive to viscosity contrast between the lithosphere and asthenospheric mantle above the rising anomaly, and the thickness of the lithosphere (Fig. 7). Higher viscosity contrasts result in amplification of the dynamic topography (Fig. 7a,b), whereas formation of a low viscosity channel reduces the dynamic topography (Fig. 7a,d). The experiments using nonlinear rheologies show local variations in viscosity, which contribute to the dynamic thinning of the mechanical lithosphere and causes reduction in dynamic topography. In addition, models using high-activation volume creates low viscosity channel above the density anomaly, which contributes decreasing the dynamic topography.

Predictions of dynamic topography derived from mantle convection models are compared against residual topography which is the component of Earth's topography that is not compensated by crustal isostasy (Flament et al., 2013; Hoggard et al., 2016). In a recent work (Cowie and Kusznir, 2018), it has been argued that dynamic topography predictions require scaling of amplitudes by ~0.75 to match with residual topography (Flament et al., 2013; Steinberger et al., 2017; Cowie and Kusznir, 2018). When density anomalies are shallower than 220 km, the misfit increases demanding a scaling factor of ~0.35 (Steinberger et al., 2017; Cowie and Kusznir, 2018). Our numerical experiments show that amplitude of dynamic topography can be nearly halved (e.g. from ~174 m in Exp. 2 to ~90 m in Exp. 5b) when we consider non-linear rheology. Therefore, we propose that part of the misfit between the dynamic topography extracted from numerical modelling of mantle convection and dynamic topography estimated from residual topography can be explained by the oversimplification of mantle viscosity in convection models. Moreover, if the density sources are shallower, the dynamic topography becomes more sensitive to the viscosity structure as has already been shown by (Morgan, 1965a; Hager and Clayton, 1989) and may lead to higher misfits.

As shown in Figure 8, uncertainties on the activation volume result in variation in dynamic topography which are higher in experiments using dry olivine rheology (i.e. 17% from an average of ~127 m) compared to experiments using wet olivine rheology (10% from an average of ~100 m). The comparison between numerical experiments using dry olivine (Exp. 4a) and wet olivine (Exp. 5b) indicates that the variation in dynamic topography can be as much as 25% from an average of ~120 m. These variations can be lessened if we have better constraints on the mantle rheology, which will advance the dynamic topography models as well as our understanding of the interaction between deep mantle and the Earth's surface.

Figures and Captions

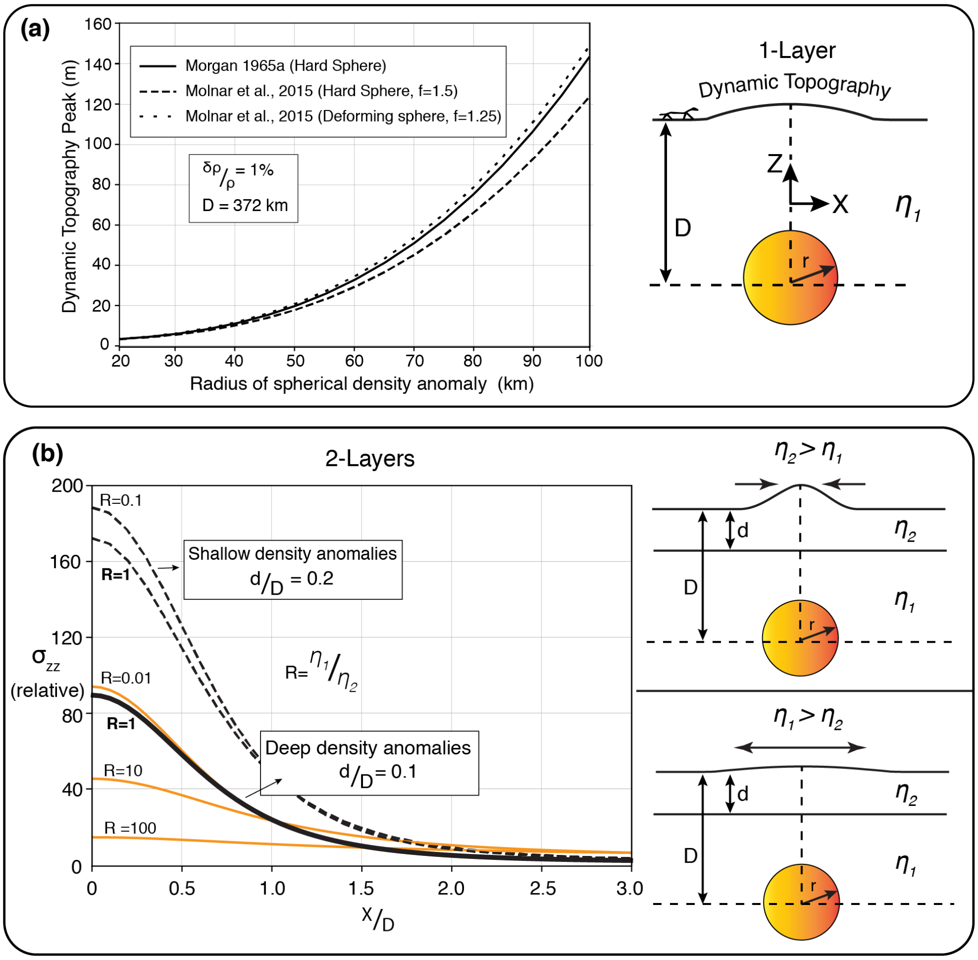

Figure 1. Dynamic topography driven by a spherical density anomaly of radius *r* at depth *D* embedded in a fluid whose viscosity structure is varied. (a) Variation in dynamic topography by radius of a spherical 1% density anomaly centred at 372 km depth in a single isoviscous fluid whose viscosity is η_1. The normal total stresses are calculated by Equation 1 in the text taken from Morgan (1965a) (hard sphere), and Equation 3 in the text taken from Molnar et al (2015) (hard and deforming spheres), and converted to dynamic topography by using Equation 2. (b) The case where the fluid

is no longer a single layer, but is composed of two layers with viscosities η_1 and η_2 for the lower and upper layers, respectively. We plot the variation in relative normal total stress at the surface in half-space due to a spherical density anomaly at a depth *D* with radius *r* by using Equation 4 in the text, taken from Morgan (1965a). The plots show relative variation in stress at a relative distance of *X/D*, for different viscosity ratio of the layers ($R=\eta_1/\eta_2$), as well as ratio of upper layer thickness to depth to the centre of the anomaly (*d/D*) of which higher values correspond to more shallow density anomalies or thicker lithosphere for constant depth (D).

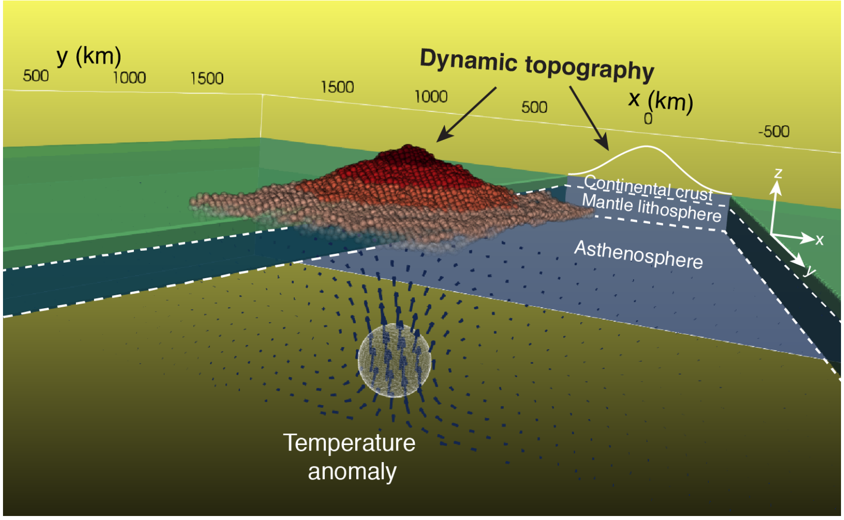

Figure 2. 3D Numerical model of a spherical temperature anomaly having 96 km radius and a density of 1% less dense than the ambient mantle embedded in a depth of 372 km. The model space is 3,840 km long in *x* and *y* axes, and 576 km deep along the *z* axis. The dynamic topography is depicted as an exaggerated surface on the top of the model and is also reflected on the *x-z* plane.

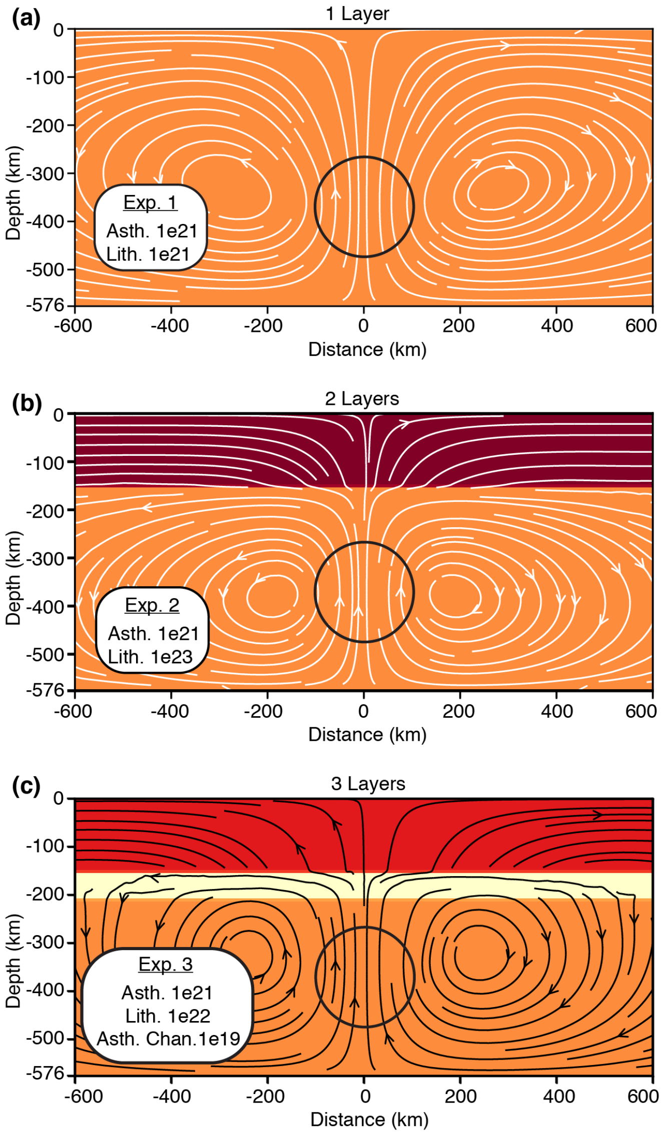

Figure 3. Viscosity map and streamlines in a 2D cross section (*x*-*z* plane) along the centre of the numerical models (*y*=0 km). All experiments include an embedded sphere with 96 km radius and centred at 372 km below the surface. The sphere (i.e. black circles) has a temperature anomaly (+324 °C) giving 1% effective density difference

with the background mantle. The ambient fluid has 1,2 or 3 isoviscous layers for Experiments 1,2 and 3 respectively.

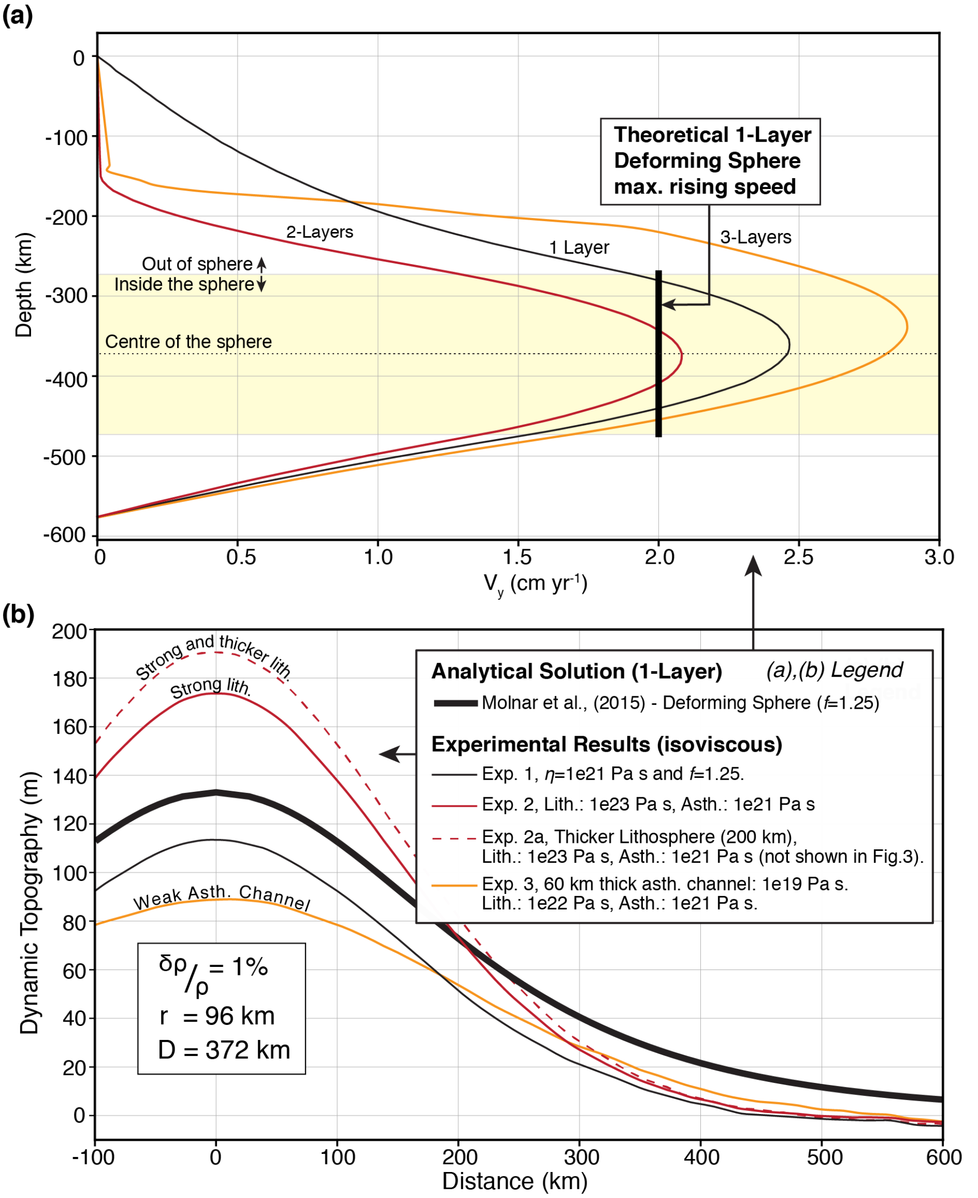

Figure 4. (a) Vertical velocity profiles (V_y) along the centre, and (b) analytical solution and numerical modelling results showing dynamic topography induced by a sphere of

temperature anomaly in the mantle (r=96 km, $\delta\rho/\rho$ = 1%). The misfit between the numerical model for R=1 and the analytical solution is due to finite space in the numerical model compared to semi-infinite space assumed in the analytical solution (Morgan 1965a).

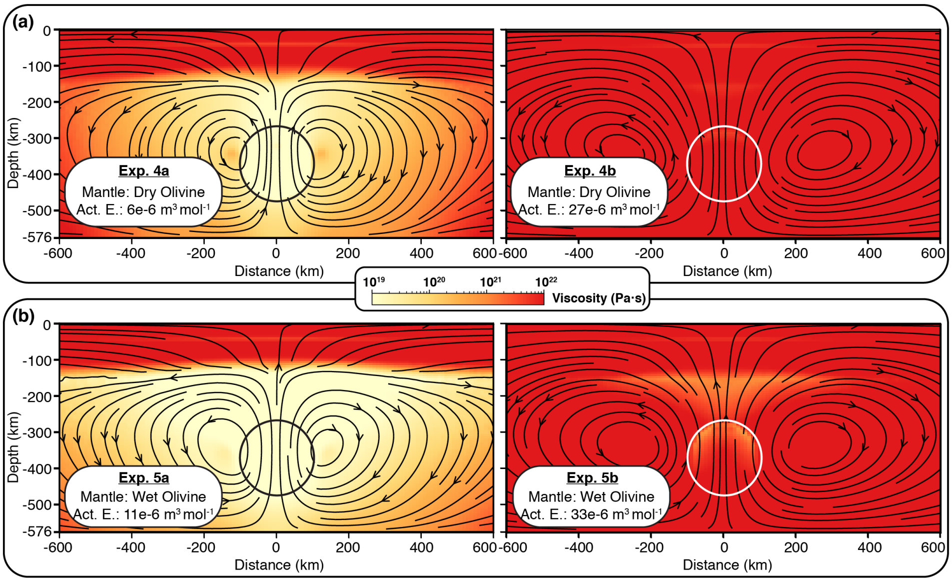

Figure 5. Viscosity map and streamlines in a 2D cross section along the centre of the numerical model (y=0) for Experiments using nonlinear rheologies for the crust and mantle. The rising sphere is shown by black or with circles in each plot. In Experiments 4 and 5, the crust and mantle has visco-plastic rheologies (see Table 1 for all parameters). The crust has dislocation creep of quartzite (Ranalli, 1995) rheology for Experiments 4a-b and Experiments 5a-b. In the mantle, the dislocation creep of dry and wet olivine rheologies are used for Experiments 4a-b and Experiments 5a-b, respectively (Hirth and Kohlstedt, 2003). For each experimental set (e.g. Experiments 4a-b), we use lowest and highest activation volumes reported for the dry or wet olivine rheology (Hirth and Kohlstedt, 2003).

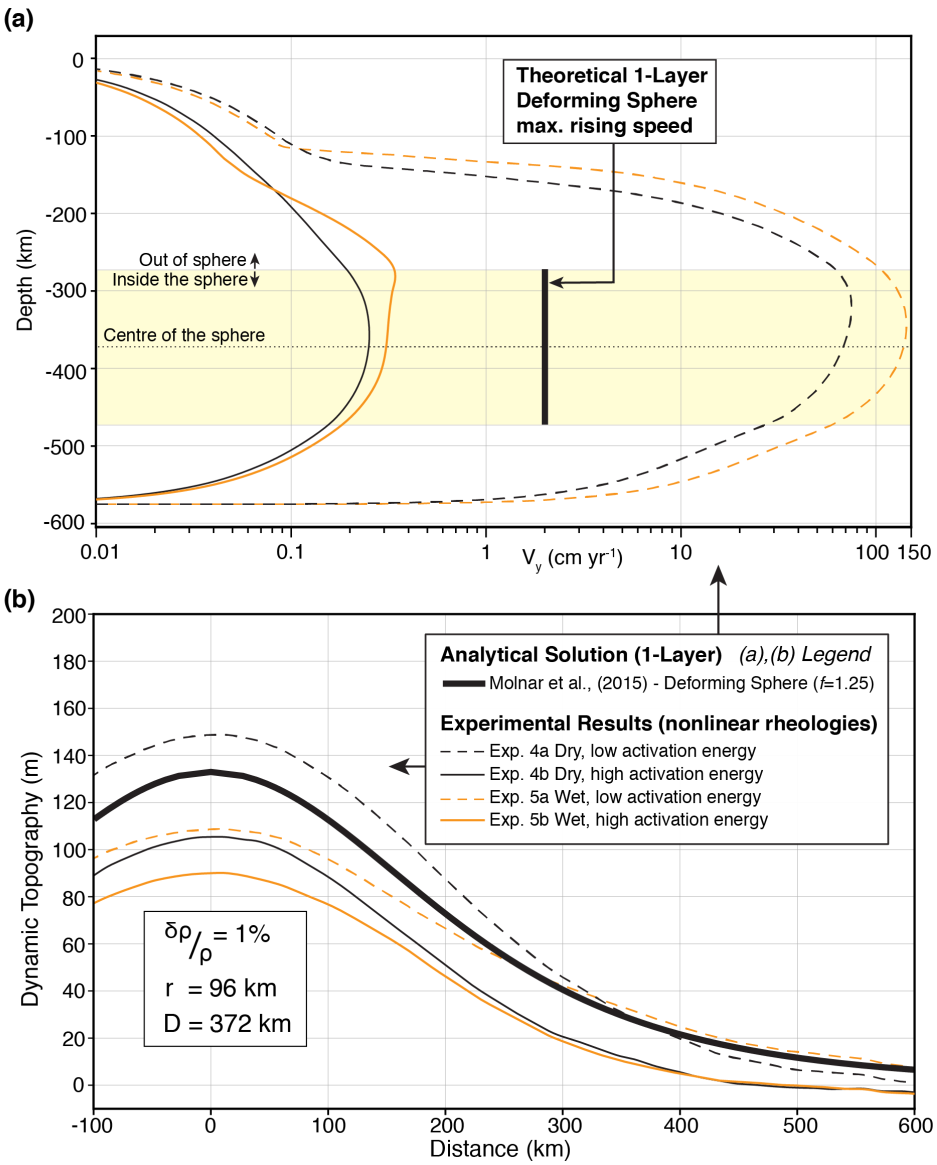

Figure 6. (a) Vertical velocity profiles (V_y) along the centre and (b) dynamic topography induced by a sphere of temperature anomaly (r=96 km, $\delta\rho/\rho$ = 1%) in the mantle that has nonlinear rheology depending on temperature, pressure and strain rate.

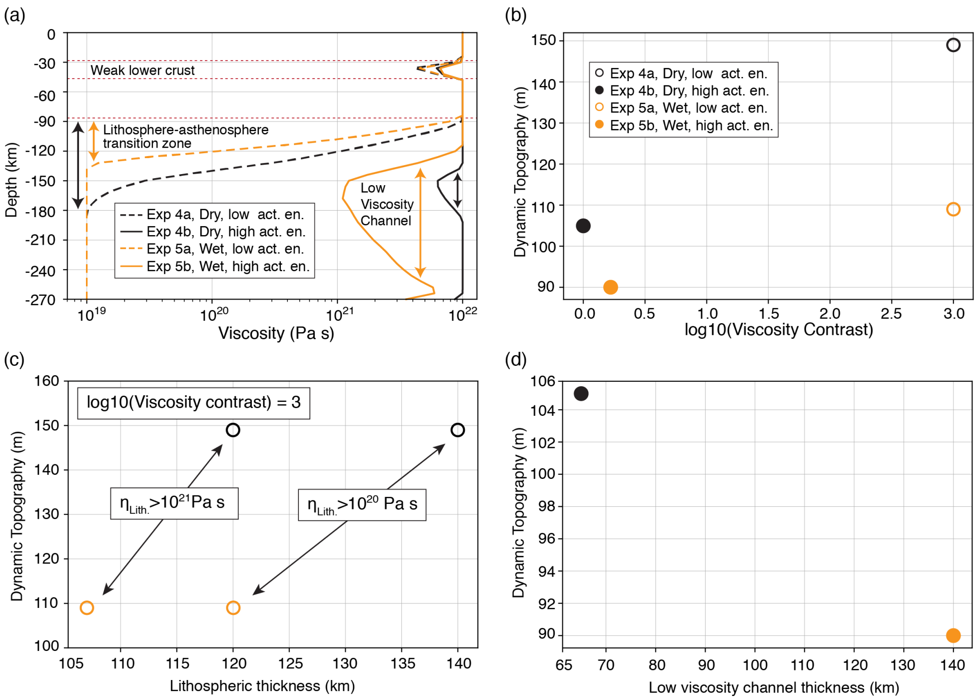

Figure 7. Important factors affecting the amplitude of dynamic topography in Experiments 4a-b and 5a-b which have nonlinear rheologies for the crust and mantle. (a) Vertical viscosity profiles at the centre of the models. Variation in dynamic topography (b) by viscosity contrast between the lithosphere and part of the asthenosphere above the spherical temperature anomaly, (c) by lithospheric thickness at constant viscosity contrast of 3 order of magnitude assuming that lithosphere-asthenosphere boundary is at 10^{20} Pa s or 10^{21} Pa s in Experiments 4a and 5a, (d) and by thickness of low viscosity channel above the spherical anomaly and beneath the lithosphere. This low viscosity channel forms only in Experiments 4b and 5b. In Experiments 4a and 5a, the viscosity profiles show progressive variation between the lithosphere and part of the asthenosphere above the spherical anomaly.

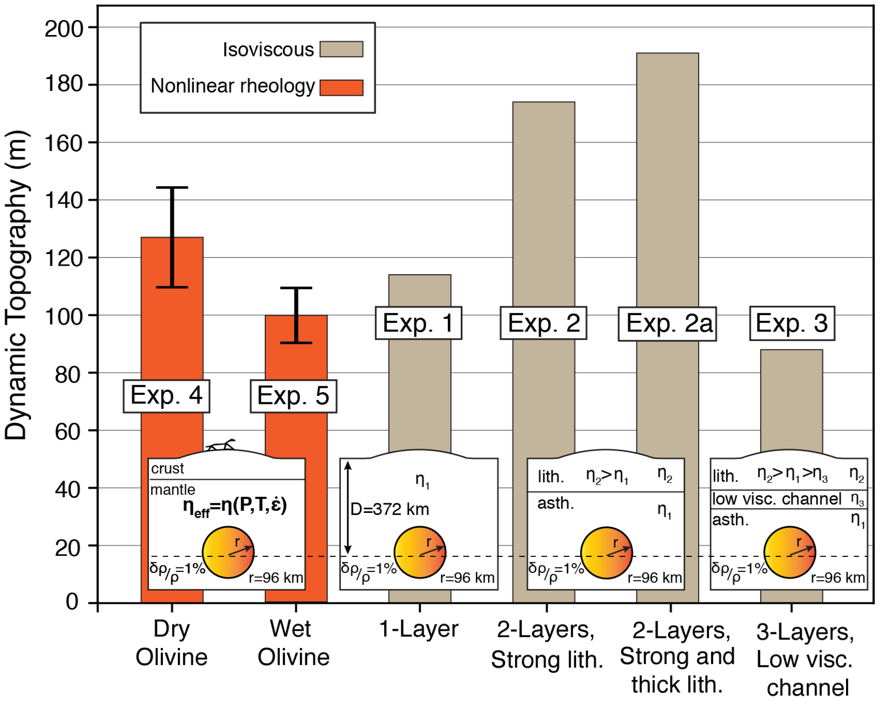

Figure 8. Compilation of predicted dynamic topographies driven by a rising sphere centred at 372 km depth with 96 km radius and 1% less denser from the ambient mantle. The difference between the experiments is either due to viscosity structure (isoviscous vs. nonlinear) in the crust and mantle or thickness of the lithosphere. We also show the model configurations for each experiment. For Experiments 4 and 5, we show variation in dynamic topography from the average of experimental results for each experimental set (e.g. Experiments 4a-b) by using error bars. These variations correspond to experiments using different activation volumes reported for dislocation creep of dry and wet olivine rheologies (Hirth and Kohlstedt, 2003). In general, experiments with nonlinear rheologies having up to 3 orders of magnitude variation in viscosity in the upper mantle (between 10^{19} Pa s and 10^{22} Pa s) generally predict lesser magnitude of dynamic topography compared to experiments using isoviscous rheology. Among the experiments using nonlinear rheologies, Experiment 5 which has wet olivine

rheology in the mantle gives lesser amplitude of dynamic topography compared to Experiment 4 which has dry olivine for the same material.

Parameters	**EXP 4a-b,5a-b Crust[1]**	**EXP 4a,4b Mantle[2]**	**EXP 5a,5b Mantle[3]**
Pre-exponential factor ($MPa^{-n} s^{-1}$)	$6.7x10^{-6}$	$1.1x10^{5}$	1600
Activation energy ($kJ mol^{-1}$)	156	530	520
Grain size exponent	0.0	0.0	0.0
Power law exponent	2.4	3.5	3.5
Water fugacity	N.A.	N.A.	1000
Water fugacity exponent	N.A.	N.A.	1.2
Activation volume ($m^3 mol^{-1}$)	0.0	$\underline{6x10^{-6}}$ or $\underline{27x10^{-6}}$	$\underline{11x10^{-6}}$ or $\underline{33x10^{-6}}$
Reference density ($kg m^{-3}$)	2,700	3,370	3,370
Reference temperature (K)	293.15	293.15	293.15
Initial cohesion (MPa)	10	10	10
Cohesion after weakening (MPa)	2	2	2
Initial coefficient of friction	0.577	0.577	0.577
Coefficient of friction after weakening	0.017	0.017	0.017
Saturation strain	0.2	0.2	0.2
Thermal diffusivity ($m^2 s^{-1}$)	$1x10^{-6}$	$1 x 10^{-6}$	$1 x 10^{-6}$
Thermal expans. (K^{-1})	$3x10^{-5}$	$3 x 10^{-5}$	$3 x 10^{-5}$
Compressibility (MPa^{-1})	$4x10^{-5}$	0	0
Heat capacity ($J K^{-1} kg^{-1}$)	1,000	1,000	1,000
Radiogenic heat production ($W m^{-3}$)	$0.5x10^{-6}$	$0.2 x 10^{-7}$	$0.2 x 10^{-7}$

Table 1. Thermal and rheological parameters for all experiments. References we are based on using the rheological parameters are (1) quartzite (Ranalli, 1995), (2) dislocation creep of dry olivine (Hirth and Kohlstedt, 2003) and (3) dislocation creep of wet olivine (Hirth and Kohlstedt, 2003). Activation volume is varied in experimental sets of 4a-b, and 5a-b.

Author contribution

Ö.F.B designed the experiments and wrote the manuscript. P.F.R. improved the manuscript and contributed in discussion of numerical modelling results.

Competing interests

The authors declare that they have no conflict of interest.

Code and data availability

In our experiments, we used Underworld, a free open-source code developed under the Australian Auscope initiative.

The version of *Underworld* code we used in our study can be found at:

https://github.com/OlympusMonds/EarthByte_Underworld

To follow an open-source philosophy and promote reproducible science, our input scripts (a suite of xml input scripts) will be available directly through the EarthByte's freely accessible web server as well as author's GitHub repository.

Acknowledgements

This research was undertaken with the assistance of resources from the National Computational Infrastructure (NCI), through the National Computational Merit Allocation Scheme supported by the Australian Government; the Pawsey Supercomputing Centre with funding from the Australian Government and the Government of Western Australia, and support from the Australian Research Council through the Industrial Transformation Research Hub grant ARC-IH130200012.

References

Becker, T. W.: Superweak asthenosphere in light of upper mantle seismic anisotropy, Geochemistry, Geophys. Geosystems, 18(5), 1986–2003, doi:10.1002/2017GC006886, 2017.

Braun, J.: The many surface expressions of mantle dynamics, Nat. Geosci., 3(12), 825–833, doi:10.1038/ngeo1020, 2010.

Cazenave, A., Souriau, A. and Dominh, K.: Global coupling of Earth surface topography with hotspots, geoid and mantle heterogeneities, Nature, 340(6228), 54–57, doi:10.1038/340054a0, 1989.

Chopra, P. N. and Paterson, M. S.: The role of water in the deformation of dunite, , 89(B9), 7861–7876, 1984.

Conrad, C. P. and Husson, L.: Influence of dynamic topography on sea level and its rate of changeInfluence of dynamic topography on sea level, Lithosphere, 1(2), 110–120, doi:10.1130/L32.1, 2009.

Cowie, L. and Kusznir, N.: Renormalisation of global mantle dynamic topography predictions using residual topography measurements for “normal” oceanic crust, Earth Planet. Sci. Lett., 499, 145–156, doi:10.1016/j.epsl.2018.07.018, 2018.

Craig, C. H. and McKenzie, D.: The existence of a thin low-viscosity layer beneath the lithosphere, Earth Planet. Sci. Lett., 78(4), 420–426, 1986.

Crough, S. T.: Hotspot swells, Annu. Rev. Earth Planet. Sci., 11(1), 165–193, 1983.

Davies, G. F. and Pribac, F.: Mesozoic seafloor subsidence and the Darwin Rise, past and present, Washingt. DC Am. Geophys. Union Geophys. Monogr. Ser., 77, 39–52, 1993.

Flament, N., Gurnis, M. and Müller, R. D.: A review of observations and models of dynamic topography, Lithosphere, 5(2), 189–210, doi:10.1130/L245.1, 2013.

Forte, A. M. and Mitrovica, J. X.: New inferences of mantle viscosity from joint inversion of long-wavelength mantle convection and post-glacial rebound data, Geophys. Res. Lett., 23(10), 1147–1150, doi:10.1029/96GL00964, 1996.

Gleason, G. C. and Tullis, J.: A flow law for dislocation creep of quartz aggregates determined with the molten salt cell, Tectonophysics, 247(1–4), 1–23, doi:10.1016/0040-1951(95)00011-B, 1995.

Gurnis, M., Mitrovica, J. X., Ritsema, J. and Van Heijst, H. J.: Constraining mantle density structure using geological evidence of surface uplift rates: The case of the African Superplume, Geochemistry, Geophys. Geosystems, 1(7), doi:10.1029/1999GC000035, 2000.

Hager, B. H.: Constraints on Mantle Rheology and Flow, J. Geophys. Res., 89(B7), 6003–6015, 1984.

Hager, B. H. and Clayton, R. W.: Constraints on the structure of mantle convection using seismic observations, flow models, and the geoid, 1989.

Hager, B. H., Clayton, R. W., Richards, M. A., Comer, R. P. and Dziewonski, A. M.: Lower mantle heterogeneity, dynamic topography and the geoid, Nature, 313(6003), 541, 1985.

Hirth, G. and Kohlstedt, D.: Rheology of the upper mantle and the mantle wedge: A view from the experimentalists, Insid. subduction Fact., 138, 83–105, 2003.

Hoggard, M. J., White, N. and Al-Attar, D.: Global dynamic topography observations reveal limited influence of large-scale mantle flow, Nat. Geosci., 9(6), 456–463, doi:10.1038/ngeo2709, 2016.

Houseman, G. A. and Hegarty, K. A.: Did rifting on Australia's Southern Margin result from tectonic uplift?, Tectonics, 6(4), 515–527, doi:10.1029/TC006i004p00515, 1987.

Isacks, B., Oliver, J. and Sykes, L. R.: Seismology and the new global tectonics, J. Geophys. Res., 73(18), 5855–5899, 1968.

Karato, S.: On the Lehmann discontinuity, Geophys. Res. Lett., 19(22), 2255–2258, 1992.

Karato, S. and Wu, P.: Rheology of the upper mantle: a synthesis., Science, 260(5109), 771–778, doi:10.1126/science.260.5109.771, 1993.

Kaufmann, G. and Lambeck, K.: Mantle dynamics, postglacial rebound and the radial viscosity profile, Phys. Earth Planet. Inter., 121(3–4), 301–324, doi:10.1016/S0031-9201(00)00174-6, 2000.

Korenaga, J. and Karato, S.: A new analysis of experimental data on olivine rheology, J. Geophys. Res. Solid Earth, 113(B2), 2008.

Mitrovica, J. X. and Forte, A. M.: Radial profile of mantle viscosity: Results from the joint inversion of convection and postglacial rebound observables, J. Geophys. Res., 102(B2), 2751, doi:10.1029/96JB03175, 1997.

Molnar, P. and Tapponnier, P.: Cenozoic tectonics of Asia: effects of a continental collision, Science (80-.)., 189(4201), 419–426, 1975.

Molnar, P., England, P. C. and Jones, C. H.: Mantle dynamics, isostasy, and the support of high terrain, J. Geophys. Res. Solid Earth, 1–26, doi:10.1002/2014JB011724, 2015.

Moresi, L., Dufour, F. and Mühlhaus, H.-B.: A Lagrangian integration point finite element method for large deformation modeling of viscoelastic geomaterials, J. Comput. Phys., 184(2), 476–497, doi:10.1016/S0021-9991(02)00031-1, 2003.

Moresi, L., Quenette, S., Lemiale, V., Mériaux, C., Appelbe, B. and Mühlhaus, H.-B.: Computational approaches to studying non-linear dynamics of the crust and mantle, Phys. Earth Planet. Inter., 163(1–4), 69–82, doi:10.1016/j.pepi.2007.06.009, 2007.

Morgan, W. J.: Gravity anomalies and convection currents: 1. A sphere and cylinder sinking beneath the surface of a viscous fluid, J. Geophys. Res., 70(24), 6175–6187, 1965a.

Morgan, W. J.: Gravity anomalies and convection currents: 2. The Puerto Rico Trench and the Mid-Atlantic Rise, J. Geophys. Res., 70(24), 6189–6204, 1965b.

Moucha, R. and Forte, A. M.: Changes in African topography driven by mantle convection, Nat. Geosci., 4, 707 [online] Available from: https://doi.org/10.1038/ngeo1235, 2011.

Moucha, R., Forte, A. M., Mitrovica, J. X., Rowley, D. B., Quéré, S., Simmons, N. A. and

Grand, S. P.: Dynamic topography and long-term sea-level variations: There is no such thing as a stable continental platform, Earth Planet. Sci. Lett., 271(1–4), 101–108, 2008.

Parsons, B. and Daly, S.: The Relationship Between Surface Topography, Gravity Anomalies, and Temperature Structure of Convection, J. Geophys. Res., 88, 1129–1144, 1983.

Pekeris, C. L.: Thermal convection in the interior of the Earth., Geophys. Suppl. Mon. Not. R. Astron. Soc., 3, 343–367, 1935.

Phipps Morgan, J., Morgan, W. J., Zhang, Y.-S. and Smith, W. H. F.: Observational hints for a plume-fed, suboceanic asthenosphere and its role in mantle convection, J. Geophys. Res. Solid Earth, 100(B7), 12753–12767, doi:10.1029/95JB00041, 1995.

Post, R. L. and Griggs, D. T.: The earth's mantle: evidence of non-Newtonian flow, Science (80-.)., 181(4106), 1242–1244, 1973.

Ranalli, G.: Rheology of the Earth, 2nd ed., Chapman & Hall, London., 1995.

Sclater, J. G. and Christie, P. A. F.: Continental stretching: An explanation of the Post-Mid-Cretaceous subsidence of the central North Sea Basin, J. Geophys. Res. Solid Earth, 85(B7), 3711–3739, doi:10.1029/JB085iB07p03711, 1980.

Steinberger, B.: Effects of latent heat release at phase boundaries on flow in the Earth's mantle, phase boundary topography and dynamic topography at the Earth's surface, Phys. Earth Planet. Inter., 164(1–2), 2–20, 2007.

Steinberger, B., Conrad, C. P., Tutu, A. O. and Hoggard, M. J.: On the amplitude of dynamic topography at spherical harmonic degree two, Tectonophysics, 2017.

Stern, R. J.: Subduction zones, Rev. Geophys., 40(December), 1031–1039, doi:10.1029/2001RG000108, 2002.

Stixrude, L. and Lithgow-Bertelloni, C.: Mineralogy and elasticity of the oceanic upper mantle: Origin of the low-velocity zone, J. Geophys. Res. Solid Earth, 110(3), 1–16, doi:10.1029/2004JB002965, 2005.